Last millennium decoupling of the South American Summer Monsoon and local hydroclimate of central Brazil

Author: Barbara E. Wortham

Last millennium decoupling of the South American Summer Monsoon and local hydroclimate of central Brazil

Barbara E. Wortham

A thesis

submitted to the Faculty of

the department of Earth and Environmental Science

in partial fulfillment

of the requirements for the degree of

Masters of Science

Boston College

Morrissey College of Arts and Sciences
Graduate School

April 2016

Last millennium decoupling of the South American Summer Monsoon and local hydroclimate of central Brazil

Barbara E. Wortham

Advisor: Corinne I. Wong, Ph.D.

Abstract

The South American Monsoon System is the dominant convective system over tropical South America during austral summer that is critical to a region heavily dependent on agricultural and hydroelectric production. An understanding of the controls on moisture conditions throughout Brazil is critical to assessing recurrent droughts and global climate change responses. An increasing number of monsoon reconstructions from $\delta^{18}O$ records provide insight into last millennium variation of regional monsoon intensity. However, the relationship between past variations in monsoon intensity and local moisture conditions has yet to be investigated. In this study, we develop speleothem $^{87}Sr/^{86}Sr$ values as a paleo-moisture proxy from a cave site located in central Brazil. Increasing speleothem $^{87}Sr/^{86}Sr$ values and decreasing $\delta^{234}U$ values over the last millennium indicate progressively wetter conditions. A similar trend in monsoon intensity is not evident in $\delta^{18}O$ records from the region, suggesting that monsoon intensity is decoupled from the local moisture conditions through the late Holocene. The potential decoupling between the monsoon and local moisture conditions suggests that processes independent from those governing monsoon intensity may play a critical role in dictating moisture variability in the region.

TABLE OF CONTENTS

List of Tables

List of Figures

Introduction

The Brazilian Cerrado (savanna) is a region with rich biodiversity and a strong agricultural economy that is sensitive to changes in climate and water availability (Franco et al., 2014). The majority of annual precipitation over the region occurs in the austral summer in association with the South American Monsoon System (SAMS). The SAMS consists of two major convective systems: insolation-driven convection centered over the southern Amazon Basin (i.e., core monsoon region) (Zhou and Lau, 1998; Vuille et al., 2012) and convergence-driven convection in the region extending from the central Amazon Basin to the South Atlantic (South Atlantic Convergence Zone, SACZ) (Lenters et al., 1999; Vera et al., 2006) (Fig. 1). Numerous studies have attempted to delineate the factors governing modern precipitation variability in the region and have sought to understand the relationship between the SACZ and the monsoon (e.g. Hastenrath and Greischar, 1993; Nogues-Paegle and Mo, 1997; Gandu and Silva Dias, 1998; Lenters et al., 1999; Chaves and Cavalcanti, 2001; Liebmann et al., 2001; Grimm, 2003; Gan et al., 2004; Grimm et al., 1998; 2007; Vera et al., 2006; Drumond et al., 2008; Dufek and Ambrizzi, 2008; Grimm and Tedeschi, 2009; Garreuad et al., 2009), but understanding of multi-decadal to centennial variability in Cerrado moisture conditions and the response of water availability to past climate change is still limited.

Existing reconstructions of SAMS intensity are largely based on $\delta^{18}O$ records (e.g. Cruz et al. 2005; 2006; 2009; Bird et al., 201; Kanner et al., 2013), which reflect both seasonality (i.e., proportion of summer monsoon vs. winter precipitation) and the degree of water vapor ^{18}O depletion (with respect to ^{16}O) due to convective activity over

the Amazon Basin (i.e., monsoon intensity) (Vuille and Werner, 2005; Vuille et al., 2012; Liu and Battisti, 2015). Although $\delta^{18}O_{precip}$ over all of Brazil is a reliable proxy of regional monsoon intensity based on the high correlation between $\delta^{18}O_{precip}$ and precipitation amount over the monsoon core region (2.5 – 7.5°S, 45 - 75°W) (Vuille and Werner 2005; Vuille et al., 2012; Brienen et al., 2012), local precipitation amount can be poorly correlated with local $\delta^{18}O_{precip}$ values at a given site (Thompson et al., 2000; Hoffman et al. 2003; Vimeux et al. 2005; Vuille and Werner 2005). Additionally, the strength and sign (i.e., positive or negative) of the correlation between monsoon intensity and precipitation amount is variable across the region and, in some areas, dependent upon the parameter from which the monsoon index is based (Fig. 2; Fig. S3). This suggests that variability in local moisture conditions, on inter-annual time scales, is not necessarily driven by variability in monsoon intensity outside of the monsoon core region. There is a large contrast between decoupling of monsoon intensity and moisture conditions over the modern interval and the strong apparent coupling of reconstructed monsoon intensity and moisture conditions in the early to late Holocene. That is, existing reconstructions of moisture conditions from vegetation and sediment records document wetter late Holocene conditions over central and southeastern Brazil relative to mid-Holocene (Stevaux, 2000; Schellekens et al., 2014; Horak-Terra et al., 2015), consistent with $\delta^{18}O$ records that document the strengthening of the monsoon from the early to late Holocene (e.g., Bird et al., 2012; Kanner et al., 2013; Thompson et al., 1995; Bird et al., 2011). The resolution, however, of existing paleo-moisture records is insufficient to assess sub-millennial variability in moisture conditions, highlighting the need for higher resolution

reconstructions of last millennial moisture conditions from monsoon-independent, moisture-sensitive proxies, which will enable assessment of the coupling between regional monsoon intensity and local moisture conditions on time scales of decades to millennia.

In this study, we develop a reconstruction of past changes in local precipitation from speleothem (TM0) $^{87}Sr/^{86}Sr$ values collected from Tamboril Cave located within the Cerrado region of central Brazil. Comparison of TM0 $^{87}Sr/^{86}Sr$ variability to $\delta^{18}O$ values in the same stalagmite and to existing paleoclimate reconstructions enables assessment of the coupling between monsoon intensity and paleo-moisture conditions over the last millennium. We find a distinct trend in TM0 $^{87}Sr/^{86}Sr$ values that evolve from the isotopic signature of the cave bedrock to the isotopic signature of soils collected above the cave. The increasing trend in $^{87}Sr/^{86}Sr$ values is interpreted to reflect decreasing water-bedrock interaction due to shorter water residence times under increasingly wetter conditions. Corresponding trends of increasing monsoon intensity are absent in last millennium monsoon reconstructions from speleothem $\delta^{18}O$ values, suggesting a decoupling between regional monsoon intensity and local moisture conditions.

Setting

Tamboril Cave (16°S, 47°W) is located in the northern part of Minas Gerais, Brazil (Fig. 1). This cave formed in the Neoproterozoic Bambui Group in the São Francisco Basin (Martins – Neto, 2009) that consists of limestones, dolomites, marls, metapelites, shales and siltstones (Carta Geologiça do Brasil, 2003). Previous studies have characterized Neoproterozoic limestones with a $^{87}Sr/^{86}Sr$ range of 0.70700 to

0.71278 (Asmerom et al., 1991; Kaufman et al., 1992; Walter et al., 2000; Thomas et al., 2004) and the Bambui limestones with a range of 0.70743 to 0.70755 (Misi and Veizner, 2006). Soils of the Cerrado region have developed *in situ* since the late Cretaceous on three distinct groups of parent material: sedimentary deposits from the river systems, gneiss and schist bedrock, and basalt flows (Marques et al., 2004). Modern climate of the Cerrado is classified as semi-humid with mean annual precipitation ranging from 958 to 1426 mm/year (Strikis et al., 2011; Silva et al., 2008), and an annual mean temperature of 22.5°C (Silva et al., 2008). Rainfall in the region is primarily controlled by the SACZ, tightly linked with the SAMS, with the majority of the precipitation occurring in the austral summer (DJF; Fig. 1a) (Vera et al., 2006; Strikis et al., 201; Moquet et al., 2016).

Materials and Methods

Soils and dripwater were collected from the cave during the dry season in July 2015 to characterize the potential $^{87}Sr/^{86}Sr$ endmembers from the cave setting (see Supplementary Material). A 50 cm pit was dug, and soils were sampled every 10-12 cm. Dripwater was collected from three sites during a single 2-3 hour interval. Soil samples were leached with 1 M ammonium acetate buffered to a pH of 8 to determine the isotopic value of the exchangeable Sr (Musgrove and Banner, 2004; Wong and Banner, 2010; Oster et al., 2010; Wong et al., 2011).

The speleothem, TM0, was collected from Tamboril Cave, at least 30 m from the entrance in a large room. TM0 is 80 cm long, generally symmetrical around a central growth axis, and consists of white aragonite needles. We recognize that inversion of speleothem aragonite to low-Mg calcite is possible during the drilling process, however,

the potential for inversion is lower in hand-milled samples and inversion has not been shown to affect trace elements (Waite and Swart, 2015). Powder subsamples (3-4 mg) were hand-milled from along the growth axis of TM0 at 0.5-1 cm resolution (average of ~20 years). Speleothem powders, soil leachates, and dripwater samples were processed using ion exchange chemistry following the methods of Montañez et al. (2000). Solution-mode multiple-collection ICP-MS analyses of strontium isotopic compositions were performed using a Nu Plasma HR instrument equipped with a DSN-100 desolvating nebulizer at the Interdisciplinary Center for Plasma Mass Spectrometry at University of California, Davis (UCD/ICPMS, n=10) and a Nu Plasma II instrument (also with DSN-100 sample introduction) at the Facility for Isotope Research and Student Training (FIRST) at Stony Brook University (n=80). Uncertainty (2σ) for analyses performed at the FIRST lab is 6.7×10^{-5} based on two standard deviations of 100 replicate analyses of the NIST SRM 987. Uncertainty for analysis performed at UCD/ICPMS is 3.3×10^{-5} based on two standard deviations of 32 replicate analyses of the NIST SRM 987 standard. The UCD/ICPMS lab also measured an internal aragonite standard (South China Sea Coral, 0.709170) that was put through ion-exchange column extraction (Sr resin) in parallel with unknowns, and the two-standard deviation of 18 replicate analyses is 2.8×10^{-5}. In both labs, analyses were drift corrected to the values of the bracketing standard, normalized to an $^{86}Sr/^{88}Sr$ value of 0.1194, and corrected for ^{84}Kr by subtracting background values. Splits of 25 samples were replicated using an IsotopX Phoenix Thermal Ionization Mass Spectrometer (TIMS) at FIRST. Uncertainty (2σ) for TIMS analyses is 6.3×10^{-6} based on 12 replicate analyses of NIST SRM 987. Differences in

samples analyzed via MC-ICPMS vs. TIMS ranged from 5.1 x 10^{-6} to 2.2 x 10^{-4}. The differences between all replicate splits were less than 1.3 x 10^{-4}, the external reproducibility of the MC-ICP-MS at FIRST (Table S2).

The age model for TM0 is based on U/Th dating of 15 distinct horizons conducted at MIT (see Supplementary Material; Table S3; Fig. S2). Speleothem powder was micromilled every 0.1 – 0.15 cm (~1-3 year resolution) and samples were analyzed for $\delta^{18}O$ using a GVI Optima IRMS at UCD and a Thermo Finnegan MAT 253 with a Kiel Device at UT. Uncertainty for $\delta^{18}O$ analyses at UCD and UT are 0.07‰ and 0.05‰, respectively, based on 64 replicate analysis of an internal standard. The TM0 stable isotope record is the focus of an independent manuscript, and will not be discussed in detail in this manuscript (Silva et al., in prep). Depth-age relationships were calculated using the COPRA algorithm (Brietenbach et al., 2012).

Results

Measured soil $^{87}Sr/^{86}Sr$ values range from 0.7309 to 0.7333 (n=4), and are substantially higher relative to limestone $^{87}Sr/^{86}Sr$ values of the Bambui Group reported in the literature (0.70743 to 0.70755; Misi and Veizner, 2006). Cave dripwater (0.7180 to 0.7223) and speleothem (0.7209 to 0.7236) $^{87}Sr/^{86}Sr$ values fall between the soil and bedrock end-members (Fig. 3inset; Table S1). Speleothem $^{87}Sr/^{86}Sr$ values increased over the last millennium (Fig. 3), gradually increasing from values closer to those of cave bedrock to values approaching those of soils overlying the cave. The initial $\delta^{234}U$ values of TM0 range from 1111 to 844 ‰ (Table S1) and decreased from the early to the late part of the last millennium.

TM0 $\delta^{18}O$ values and existing $\delta^{18}O$ records from the region, in contrast, do not exhibit long-term trends over the last millennium (Fig. 3). Rather, existing $\delta^{18}O$ records exhibit distinct multi-centennial variation widely interpreted to reflect a weaker monsoon during the Medieval Climate Anomaly (MCA) and/or stronger monsoon during the Little Ice Age (LIA) (Thompson et al., 1995; Seltzer et al., 2000; Pollisar et al., 2006; vanBreukelen et al., 2008; Reuter et al., 2009; Bird et al., 2011; Vuille et al., 2012; Kanner et al., 2013).

Discussion

Speleothem $^{87}Sr/^{86}Sr$ values as a moisture proxy

Variations in TM0 $^{87}Sr/^{86}Sr$ values likely reflect changing amounts of water-rock interaction in response to variations in moisture conditions, similar to previous speleothem $^{87}Sr/^{86}Sr$ time series that have been developed as proxies of paleoclimate conditions. In regions where soil and bedrock have distinct $^{87}Sr/^{86}Sr$ signatures, dripwater and speleothem $^{87}Sr/^{86}Sr$ values generally reflect varying durations of contact with the host bedrock associated with varying water residence time (Banner et al., 1994; 1996; Bar-Matthews et al., 1999; Musgrove and Banner, 2004; Oster et al., 2009; Wong and Banner, 2010; Wong et al., 2011; Vaks et al., 2013). That is, infiltrating waters acquire an initial $^{87}Sr/^{86}Sr$ signature from the soil overlying the cave, which then progressively evolves toward the $^{87}Sr/^{86}Sr$ signature of the host carbonate bedrock (Fig. S1). Previous numerical modeling of contemporary cave dripwater and groundwater $^{87}Sr/^{86}Sr$ compositions in Texas and in California are consistent with relatively shorter water residence times, due to relatively wetter conditions and/or more conduit- (vs. diffuse-)

dominant flow-paths, limiting the extent of water-rock interaction and the evolution of the isotopic signature toward the bedrock end-member (Musgrove and Banner, 2004; Oster et al., 2010; Wong et al., 2011). Lastly, speleothem $^{87}Sr/^{86}Sr$ variability can additionally reflect variations in dust flux in settings where proximal dust sources have distinct isotopic signatures relative to the cave site. Variations in dust flux, as tracked by speleothem $^{87}Sr/^{86}Sr$ values, can serve as a proxy for changes in atmospheric circulation as is the case in China (Goede et al., 1998; Li et al., 2005; Zhou et al., 2009), or aridity in the dust source region, as in the case of Israel (Frumkin and Stein, 2004).

We argue that TM0 speleothem $^{87}Sr/^{86}Sr$ values reflect paleo-moisture conditions and likely reflect a trend of increasing water availability over the last millennium. Cave dripwater and TM0 $^{87}Sr/^{86}Sr$ values lie between by endmember soil and bedrock $^{87}Sr/^{86}Sr$ values, consistent with the interpretation that the isotopic signature of infiltrating water evolves via water-rock interaction from that initially acquired from the soil toward that of the host bedrock (Fig. S1). Furthermore, TM0 $^{87}Sr/^{86}Sr$ variations cannot be accounted for by variations in dust flux as discussed below.

It is unlikely that aerosol dust deposition played an influential role in $^{87}Sr/^{86}Sr$ variability of TM0. It is well known that African dust is transported across the Atlantic to South America during the austral summer (e.g., Koran et al., 2006; Ben-Ami et al., 2010). Although no studies specifically investigate dust deposition in the region of Tamboril Cave, several studies provide prospective on the relative contribution of Saharan dust to regions further north in the Amazon Basin that receive the largest fluxes (Koran et al., 2006; Ben-Ami et al., 2010). Saharan dust does not appear to contribute substantial

amounts of Sr to regional soils as i) African dust and Amazonian deposits have distinct Pb-Nd-Sr isotopic signatures (Abouchami et al., 2013; Pourmand et al., 2014), ii) the composition of Amazonian deposits is consistent with in-situ weathering and erosion of the Precambrian Amazon craton (Abouchami et al., 2013), and iii) vertical erosion rates dwarf aeolian accumulation rates at the core of the Brazilian monsoon region (Abouchami et al., 2013). Additionally, recent work suggests that the boreal summer African dust plume has been stable over the last 2 ka (Hayes et al., submitted), which may also suggest stability in the winter dust plume as the strength of summer and winter dust plumes tends to co-vary (Grousset et al., 1998; Moreno et al., 2000; Ridley et al., 2014; Williams et al., submitted). Given the limited influence of Saharan dust on the isotopic composition of surface material in the region of greatest dust flux and the stability of the dust flux over the last 2 ka, it is unlikely that Saharan dust played a role in evolving TM0 $^{87}Sr/^{86}Sr$ values over the last millennium.

Decreasing TM0 $\delta^{234}U$ values are also consistent with our interpretation of increasingly wetter conditions over the last millennium at Tamboril Cave (Fig. 4). Speleothem $\delta^{234}U$ values are directly inherited from the drip-water they precipitate from, and drip-water $\delta^{234}U$ values evolve as a product of water residence time. Infiltrating water acquires an initial $\delta^{234}U$ signature from the surface material with which it first interacts (e.g. soil or soil carbonates), which, if sufficiently old (> 1 million years), is typically depleted in ^{234}U with respect to ^{238}U relative (i.e., $\delta^{234}U > 10^6$ years; Oster et al., 2012). Relatively longer water transit times from the surface to the cave results in higher $\delta^{234}U$ values as infiltrating water accumulates ^{234}U due to the combination of

preferentially leaching of ^{234}U from damaged lattice sites within the bedrock and the ejection of ^{234}Th (which decays to ^{234}U) from the bedrock associated with ^{238}U decay via α-recoil. Conversely, lower $\delta^{234}U$ values reflect shorter water residence time and more limited extents of water-rock interaction (as driven by higher infiltration rates) (Ayalon et al., 1999; Bar-Matthews et al., 1999; Frumkin and Stein, 2004; Zhou et al., 2005; Griffiths et al., 2010; Polyak et al., 2012; Oster et al., 2012). The stepped nature of TM0 $\delta^{234}U$ values, relative to the more progressive evolution of $^{87}Sr/^{86}Sr$ values, suggests varying sensitivity of these two proxies to changing moisture conditions. Differences in sensitivity between the proxies could be an artifact of the differences in sampling resolution, i.e., $\delta^{234}U$ was measured at lower resolution, relative to $^{87}Sr/^{86}Sr$ values, thus the nature of the transition is less clearly resolved. Alternatively, $\delta^{234}U$ values have been found to be invariant when speleothem growth rates relatively fast and $\delta^{234}U$ values are near secular equilibrium ($^{234}U/^{238}U_o \sim 0.7\text{-}1.0$), suggesting that sufficiently short transit times severely limit the evolution of dripwater $\delta^{234}U$ values (Zhou et al., 2005). This is consistent with the TM0 records, which show an increase in growth rate towards the present (Table S1) and a stability of the $\delta^{234}U$ record over the last millennium.

Decoupling of monsoon intensity and Cerrado hydroclimate

TM0 and regional $\delta^{18}O$ records do not reflect a similar long-term shift in the intensity of the monsoon (Fig. 2), suggesting the influence of non-monsoon related processes on the local moisture conditions. Measured $\delta^{18}O_{precip}$ values across the region reflect the intensity of convection over the southern Amazon Basin that drives the summer monsoon, but are not necessarily a reliable proxy of precipitation amount at a

given site throughout the tropical to subtropical South American region (Vuille et al., 2012). Although last millennium $\delta^{18}O$ records from the region document distinct centennial variability in regional monsoon intensity (e.g. Bird et al., 201; Kanner et al., 2013), these records do not suggest a progressive intensification of the monsoon over this same time period that could account for the wetting trend indicated by the TM0 $^{87}Sr/^{86}Sr$ record. A lack of co-variation between local moisture conditions and regional monsoon intensity over the last millennium could indicate the decoupling of the convective systems associated with the SAMS. Considering that central Brazil lies within the direct influence of the South Atlantic Converge Zone (SACZ) (Liebmann et al., 1999; Strikis et al., 201; Moquet et al., 2016) it is possible that variability in the position or intensity of the SACZ is independent of variations in convective intensity over the Amazon Basin.

Investigations of modern and past climate suggest that variability in monsoon intensity is driven by climate dynamics distinct from those governing the position and strength of the SACZ. Modern climate simulations document the production of a Rossby wave train in response to El Nino and La Nina events that results in a dipole pattern of convective activity across South America, enhancing convection over the Amazon Basin during an El Nino while suppressing convection over the SACZ (Grimm, 2003; Garreaud et al., 2009). Both modern climate simulations and paleoclimate reconstructions suggest that the position of the Intertropical Convergence Zone shifts in response to variations in Tropical Atlantic sea surface temperatures (SSTs), which modulates the intensity of monsoon convection (REFS) The mean position and strength of the SACZ, however, is dictated by variability in subtropical South Atlantic SSTs (e.g. Barros, 2000; Doyle and

Barros, 2002; Chaves and Nobre, 2004; de Almeida et al., 2007). Lastly, paleoclimate simulations delineate distinct climate dynamics governing the responses of the SAMS convective zones to orbital (precessional) variability in insolation. Comparison of high- (207ka) and low- insolation (218 ka) climate simulations (difference of 90 W/m^2 at 30°S) document that variations in insolation drive variability in differential land-ocean heating that modulates convective activity over the Amazon basin. The response of the SACZ to insolation differences, however, results a Rossby wave train associated with shifts in temperature and moisture conditions over southern Africa (Liu and Battisti, 2015). Although these studies span different temporal scales and forcing mechanisms, these studies provide evidence that convection over the Amazon Basin and SACZ can be influenced by distinct climate processes, and, in some cases, drive the decoupling of monsoon intensity from local (central Brazil) moisture conditions.

Output from the last millennium climate ensemble simulation using the Community Earth System Model (Otto-Bleisner et al., 2015) seemingly could provide additional insight into the potential decoupling of the monsoon and SACZ convective systems. These lack an obvious precipitation (and evapo-transpiration) trend in central Brazil and do not capture the variability of monsoon intensity during the MCA and LIA (Sup Figs. 4, 5). The inconsistency between model results and climate proxies suggests that the simulation does not capture all factors associated with atmospheric dynamics, which are critical to last millennium moisture conditions over subtropical South America (Landrum et al., 2013).

The contrast between the TM0 reconstruction of local moisture conditions and existing reconstructions of regional monsoon intensity could alternatively reflect the influence of local water dynamics unrelated to the SAMS. For instance, our record could be influenced by austral winter precipitation, a potentially plausible explanation considering austral winter (JJA) precipitation accounts for 40% of the annual precipitation in the modern climate. A decrease in evapotranspiration could account for increasing water availability inferred from the TM0 $^{87}Sr/^{86}Sr$ record. However, paleovegetation reconstructions from the region document the expansion of woodland forest over savanna during the late Holocene (Silva et al., 2008). Although forest encroachment is expected to both suppress evaporation and increase transpiration, a transition from open savanna to woodland likely increased rather than decreased evapotranspiration locally. Furthermore, such shifts in vegetation distribution are generally interpreted as a response to (not driver of) wetter conditions in corroboration of the effective moisture trend inferred from paleo-vegetation records in many parts of South America (Silva, 2014). It is evident that additional work is necessary to resolve the mechanism(s) driving the apparent decoupling between last millennium moisture conditions and monsoon intensity in central Brazil. Future studies stand to gain valuable information by including additional paleo-moisture records from the region and plant-derived records of water availability (Silva, 2015; Silva et al., 2015), which are needed to understand the impact of climate variability on terrestrial ecosystems.

Conclusions

Our current understanding of how and why moisture conditions varied over central Brazil over the last millennium is limited and relies on monsoon reconstructions, for which the coupling to local moisture conditions has yet to be rigorously assessed. We developed a last millennium speleothem $^{87}Sr/^{86}Sr$ record that documents the evolution of $^{87}Sr/^{86}Sr$ values from the isotopic signature of the bedrock towards that of the soil, which is interpreted to reflect decreasing water-rock interaction due to increasing moisture availability in central Brazil. This interpretation is consistent with decreasing $\delta^{234}U$ values in the same speleothem, suggesting wetter conditions. A similar trend in existing $\delta^{18}O$ reconstructions of monsoon intensity is lacking, highlighting a decoupling between regional monsoon intensity and local moisture conditions. Determining the drivers of spatial and temporal variability in local moisture conditions is critical to assess the degree to which moisture is coupled to regional monsoon intensity and the vulnerability of moisture conditions to global climate change.

References

Asmerom,Y., Jacobsen, S.B., Knoll, A.H., Butterfield, N.J., and Swett, K. 1991. Strontium isotopic variations of Neoproterozoic seawater: Implications for crustal evolution. *Geochimica et Cosmochimica Acta*. 55:2883-2894.

Ayalon, A., Bar-Matthews, M., and Kaufman, A. 1999. Petrography, strontium, barium and uranium concentrations, and strontium and uranium isotope ratios in speleothems as paleoclimatic proxies: Soreq Cave, Israel. *The Holocene*. 9,6:715-722.

Banner, J. L., Musgrove, M., Edwards, R. L., Asmerom, Y., and Hoff, J. A. 1996. High-resolution temporal record of Holocene ground-water chemistry: Tracing links between climate and hydrology. *Geology*. 24: 1049-1052.

Banner, J. L., Musgrove, M., and Capo, R. 1994. Tracing groundwater evolution in a limestone aquifer using Sr isotopes - Effects of multiple sources of dissolved ions and mineral-solution reactions. *Geology* . 22: 687-690.

Bar-Matthews, M., Ayalon, A., Kaufman, A., and Wasserburg, G.J. 1999. The Eastern Mediterranean paleoclimate as a reflection of regional events: Soreq cave, Israel. *Earth and Planetary Science Letters*. 166:85-95.

Barreiro, M., Chang, P. and Saravanan, R. 2002. Variability of the South Atlantic Convergence Zone Simulated by an Atmospheric General Circulation Model. *Journal of Climate*.15: 745–763.

Breitenbach, S.F.M., Rehfeld, K., Gowwami, B., Baldini, J.U.L., Ridley, H.E., Kennett, D.J., Prufer, K.M., Aquino, V.V., Asmerom, Y., Polyak, V.J., Cheng, H., Kurths, J., and Marwan, N. 2012. Constructing Proxy Records from Age models (COPRA). *Climate of the Past*. 8: 1765-1779.

Bird, B.W., Abbot, M.B., Vuille, M., Rodbell, D.T., Stansell, N.D., and Rosenmeier, M.F. 2011. A 2300-year-long annually resolved record of the south American summer monsoon from the Peruvian Andes. *Proc. Nat. Academy of Sciences*. 108(21):8583-8588.

Brienen, R. J. W.,Helle, G.. Pons, T. L, Guyot, J.-L. and Gloor, M. 2012 Oxygen isotopes in tree rings are a good proxy for Amazon precipitation and El Nino-Southern Oscillation variability. *Proc. Nat. Academy of Sciences* .109(42): 16957-16962.

Cruz, F.W., Burns, S.J., Karmann, I., Sharp, W.D., Vuille, M., Cardoso, A.O., Ferrari, J.A., Silva Dias, P.L., and Viana, O. Jr. 2005. Insolation-driven changes in atmospheric circulation over the past 116,000 years in subtropical Brazil. *Nature*. 434:63-65.

Dai, A. 2006. Precipitation Characteristics in Eighteen Coupled Climate Models. *Journal of Climate*. 19:4605-4630.

De Almeida, R.A.F., Nobre, P., Haarsma, R.J., Campos, E.J.D. 2007. Negative ocean-atmosphere feedback in the South Atlantic Convergence Zone. *Geophysical Research Letters*. 34:L18809.

Franco et al (2014). Cerrado vegetation and global change: the role of functional types, resource availability and disturbance in regulating plant community responses to rising CO2 levels and climate warming. *Theoretical and Experimental Plant Physiology*, *26*(1), 19–38. http://doi.org/10.1007/s40626-014-0002-6

Serviço Geológico do Brasil (CPRM). 2003. State Geologic Maps: Minas Gerais. http://geobank.cprm.gov.br/pls/publico/geobank/

Hayes C.T., D. McGee, E.A. Boyle, S. Mukhopadhyay, A.C. Maloof. Stable deposition of African dust to the Bahamas over recent millennia. Submitted to *J. Geophysical Research-Atmospheres*, Feb. 2016.

Hoffman, G., Ramirez, E., Taupin, J.D., Francou, B., Ribstein, P., Delmas, R., Durr, H., Gallaire, R., Simoes, J., Schotterer, U., Stievenard, M., and M. Werner. 2003. Coherent isotope history of Andean ice cores over the last century. *Geophysical Research Letters*. 30(4): 1179.

Kanner, L.C, Burns, S.J., Cheng, H., Edwards, R.L., and Vuille, M. 2013. High-resolution variability of the South American summer monsoon over the last seven millennia: insights from a speleothem record from the central Peruvian Andes. *Quaternary Science Reviews*. 75: 1-10.

Kaufman, A.J., Knoll, A.H., and Awramik, S.M. 1992. Biostratigraphic and chemostratigraphic correlation of Neoproterozoic sedimentary successions: Upper Tindir Group, northwestern Canada, as a test case. *Geology.* 20:181-185.

Landrum, L., Otto-Bleisner, B.L., Wahl, E.R., Conley, A., Lawrence, P.J., Rosenbloom, N., and Teng, H. 2013. Last Millennium Climate and Its Variability in CCSM4. *Journal of Climate*. 26:1085-1108.

Liebmann, B., Kiladis, G.N, Marengo, J.A., Ambrizzi, T., Glick, J.D. 1999. Submonthly convective variability over South America and the South Atlantic Convergence Zone. *Journal of Climate.* 12.7:1877-1891.

Liu, X., and Battisti, D.S., The influence of orbital forcing of tropical insolation on the climate and isotopic composition of precipitation in South America. *Journal of Climate*. 28(12): 4841-4862.

Malhi, Y., Aragäo, L.E.O.C., Galbraith, D., Huntingford, C., Fisher, R., Zelazowski, P., Sitch, S., McSweeney, C., Meir, P. and Schellnhuber, H. J. Exploring the Likelihood and Mechanism of a Climate-Change-Induced Dieback of the Amazon Rainforest. *Proc. Nat. Acad. Sciences.* 106(49): 201610-20615.

Martins-Neto, M.A. 2009. Sequence stratigraphic framework of Proterozoic successions in eastern Brazil. *Marine and Petroleum Geology*. 26(2) 163-176.

Misi, A., Kaufman, A.J., Veizer, J., Powis, K., Azmy, K., Boggiani, P.C., Gaucher, C., Teixeira, J.B.G., Sanches, A.L., and Iyer, S.S.S. 2007. Chemostratigraphic correlation of Neoproterozoic succession in South America. *Chemical Geology*. 237:143-167.

Moquet, Js., Cruz, F.W., Novello, V.F., Strikis, N.M, Deininger, M., Karmann, I., Ventura Santos, R., Millot, C., Apaestegui, J., Guyot, J.-L., Siffedine, A., Vuille, M., Cheng, H., Edwards, R.L., and Santini, W. 2016. Calibration of speleothem d18O records against hydroclimate instrumental records in Central Brazil. *Global and Planetary Change*.

Montañez, I. P., Osleger, D. A., Banner, J. L., Mack, L. E., and Musgrove, M. 2000. Evolution of the Sr and C isotope composition of Cambrian oceans. *GSA Today.* 10(5): 1-5.

Musgrove, M. and Banner, J. L. 2004. Controls on the spatial and temporal variability of vadose dripwater geochemistry: Edwards Aquifer, central Texas. *Geochimica et Cosmochimica Acta*. 68: 1007-1020.

Novello, V.F., Cruz, F.W., Karmann, I., Burns, S.J., Strikis, N.M., Vuille, M., Cheng, H., Edwards,R.L., Santos, R.V., Frigo, E., Barreto, E.A.S. 2012. Multidecadal climate variability in Brazil's Nordeste during the last 3000 years based on speleothem isotope records. *Geophyscial Research Letters*. 39: L23706

Oster, J.L., Montañez, I.P., Guilderson, T.P., Sharp, W.D., and Banner, J.L. 2010. Modeling speleothem d13C variability in a central Sierra Nevada cave using 14C and 87Sr/86Sr. *Geochimica et Cosmochimica Acta*. 74: 5228-5242.

Polissar, P.J., Abbott, M.B., Shemesh, A., Wolfe, A.P., and Bradley, R.S. 2006. Holocene hydrologic balance of tropical South America from oxygen isotopes of lake sediment opal, Venezuelan Andes. *Earth and Planetary Science Letters*. 242: 375 - 389.

Reuter, J., Stott, L., Khider, D., Sinha, A., Cheng, H., and Edwards, R.L. 2009. A new perspective on the hydroclimate variability in northern South America during the Little Ice Age. *Geophyscial Research Letters*. 36: L21706.

Ridley, D.A., Heald, C.L., Prospero, J.M., 2014. What controls the recent changes in African mineral dust aerosol across the Atlantic? *Atmos. Chem. Phys.* 14, 5735–5747. doi:10.5194/acp-14-5735-2014

Seltzer, G., Rodbell, D., and Burns, S. 2000. Isotopic evidence for late Quaternary climatic change in tropical South America. *Geology*. 28(1): 35-38.

Silva, L. C. R. (2014). Importance of climate-driven forest–savanna biome shifts in anthropological and ecological research. Proceedings of the National Academy of Sciences of the United States of America, 111(37), E3831–E3832. http://doi.org/doi/10.1073/pnas.1413205111

Silva, L. C. R., Pedroso, G., Doane, T. A., Mukome, F. N. D., & Horwath, W. . (2015). Beyond the cellulose: Oxygen isotope composition of plant lipids as a proxy for terrestrial water balance. Geochemical Perspective Letters, 1, 33–42.

Silva, L. C. R. (2015). From air to land: understanding water resources through plant-based multidisciplinary research. Trends in Plant Science, 20(7), 399–401. http://doi.org/10.1016/j.tplants.2015.05.007

Silva, L.C.R., and Anand, M. 2011. Mechanisms of Araucaria (Atlantic) Forest Expansion into Southern Brazilian Grasslands. *Ecosystems*. 14: 1354-1371.

Silva, L.C.R., Sternberg, L., Haridasan, M., Hoffmann, W.A., Miralles-Wilhelm, F., and Franco, A.C. 2008. Expansion of gallery forests into central Brazilian savannas. *Global Change Biology*. 14: 2108-2118.

Strikis, N.M., Cruz, F.W., Cheng, H., Karmann, I., Edwards, R.L., Vuille, M., Wang, X., de Paula, M.S., Novello, V.F., and Auler, A.S. 2011. Abrupt variations in South American monsoon rainfall during the Holocene based on a speleothem record from central-eastern Brazil. *Geology*. 39(11):1075-1078.

Swap, R. Garstang, M., Greco, S., Talbot, R., and Kallberg, P.1992. Saharan dust in the Amazon Basin. *Tellus*. 44B:133-149.

Thomas, C.W., Graham, C.M., Ellam, R.M., and Fallick, A.E. 2004. 87Sr/86Sr chemostratigraphy of Neoproterozoic Dalradian limestones of Scotland and Ireland: constraints on depositional ages and time scales. *Journal of the Geological Society, London*. 161: 229-242.

Thompson, L.G., Mosley-Thompson,E., Davis, M.E., Lin, P.-E., Henderson, K.A., Cole-Dai, J., Bolzan, J.F., Liu, K.-b. 1995. Late glacial stage and Holocene tropical ice core records from Huascaran, Peru. *Science*. 269:46-50.

Thompson, L.G., Mosley-Thompson, E., and Henderson, K.A. 2000. Ice-core paleoclimate records in tropical South America since the Last Glacial Maximum. *Journal of Quaternary Science*. 15(4): 377-394.

Vaks, A., Woodhead, J., Bar-Matthews, M.., Ayalon, A., Cliff, R.A., Zilberman, T., Matthews, A., and Frumkin, A. 2013. Pliocene-Pleistocene climate of the northern margin of Saharan-Arabian Desert recorded in speleothems from the Negev Desert, Israel. *Earth and Planetary Science Letters*. 368:88-100.

Van Breukelen, M.R., Vonhof, H.B., Hellstrom, J.C., Wester, W.C.G., and Kroon, D. 2008. Fossil dripwater in stalagmites reveals Holocene temperature and rainfall variation in Amazonia. *Earth and Planetary Science Letters*. 275: 54-60.

Vera, C., Higgins, W., Amador, J., Ambrizzi, T., Garreaud, R., Gochis, D., Gutzler, D., Lettenmaier, D., Marengo, J., Mechoso, C.R., Nogues-Paegle, J., Silva Dias, P.L., and Zhang, C. 2006. Toward a unified view of the American monsoon systems.

Vimeux, F., Gallaire, R., Bony, S., Hoffman, G., and Chiang, J.C.H. 2005. What are the climate controls on dD in precipitation in the Zongo Valley (Bolivia)? Implications for the Illimani ice core interpretation. *Earth and Planetary Science Letters*. 240: 205-220.

Vuille, M., and Werner, M. 2005. Stable isotopes in precipitation recording South American summer monsoon and ENSO variability: observations and model results. *Climate Dynamics*. 25:401-413. *Journal of Climate*. 19: 4977-5000.

Vuille, M., Burns, S.J., Taylor, B.L., Cruz, F.W., Bird, B.W., Abbott, M.B., Kanner, L.C., Cheng, H., and Novello, V.F. 2012. A review of the South American monsoon history as recorded in stable isotopic proxies over the past two millennia. *Climate of the Past*. 8:1309-1321.

Walter, M.R., Veevers, J.J., Calver, C.R., Gorjan,P., and Hill A.C. 2000. Dating the 840-544 Ma Neoproterozoic interval by isotopes of strontium, carbon, and sulfur in seawater, and some interpretative models. *Precambrian Research*. 100:371-433.

Williams R.H., D. McGee, D.A. Ridley, C.W. Kinsley, S. Hu, A. Fedorov, I. Tal, R. Murray, P.B. deMenocal. Glacial to Holocene changes in trans-Atlantic Saharan dust transport and dust-climate feedbacks. Submitted to *Science Advances*, Feb. 2016.

Wong, C.I. and Banner, J.L. 2010. Response of cave-air CO2 and drip-water to brush clearing in central Texas: implications for recharge and soil CO2 dynamics. *Biogeosciences*. 115: G04018.

Wong, C.I., Banner, J.L., Musgrove, M. 2011. Seasonal dripwater Mg/Ca and Sr/Ca variations driven by cave ventilation: implications for and modeling of speleothem paleoclimate records. *Geochimica et Cosmochimica Acta*. 75: 3514-3529.

Figures

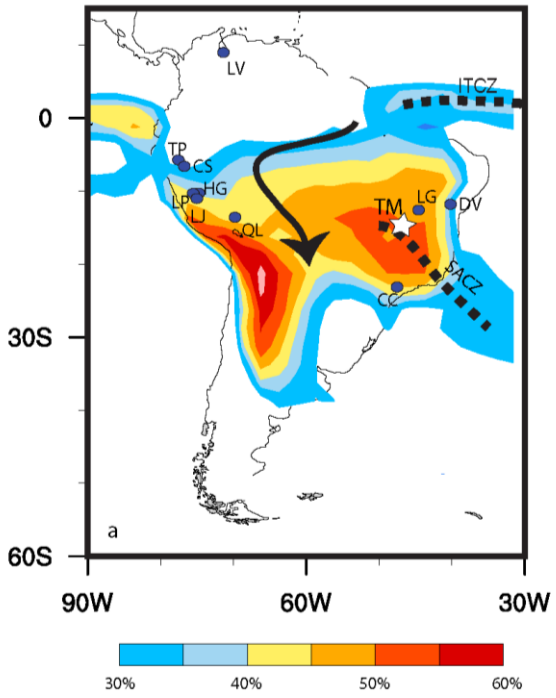

Figure 1: SAMS precipitation patterns over study region (a) Shading reflects average austral summer (DJF) precipitation as a percentage of the annual precipitation (data spanning 1981-2010 from Global Precipitation Climatology Project). Locations of exisiting late Holocene paleo-SASM reconstructions with decadal to subdecadal resolution indicated by circles (Andean Sites: HG-Huagapo Cave, CS-Cascayunga Cave,TP-Tigre Perdido Cave, LP-Lake Pumacocha, LJ-Lake Junin, QC-Quelccaya Ice Cap. Also shown: CC-Cristal Cave, LG-Lapa Grande Cave, DV-Diva de Maura record, and LV-Lake Verdes Alta and Baja). The mean positions of the ITCZ and the SACZ during DJF are shown as black dashed lines. Star indicates the location of the study site,

Tamboril Cave (TM). Black arrow represents the easterly transport of moisture across the Amazon Basin, and subsequent deflection of winds to the south by the Andean Mountain range creating the South American low-level jet.

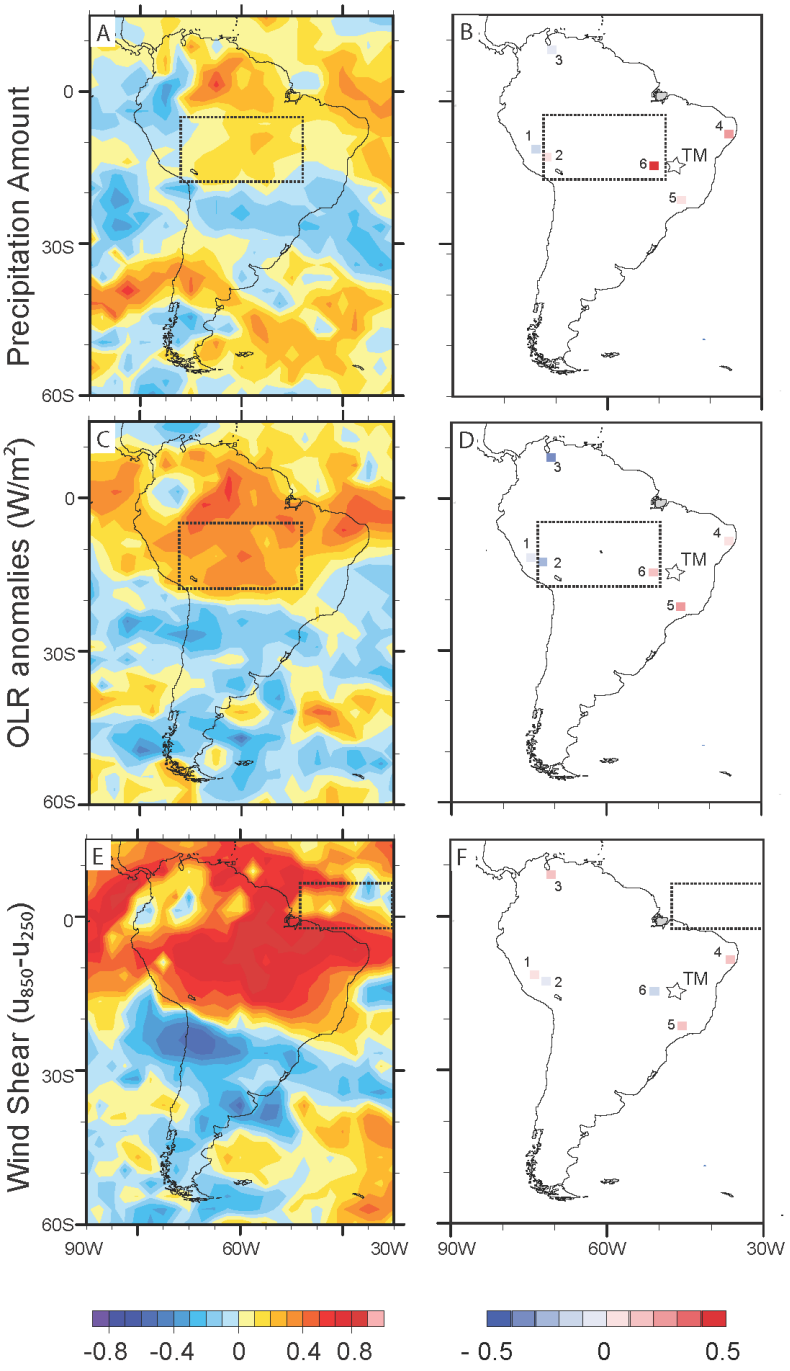

Figure 2: Correlations between three unique indices of monsoon intensity and gridded precipitation (Climate Prediction Center Merged Analysis of Precipitation; A, C, E) and precipitation guage (squares; B, D, F) data across South America for the interval of 1979-2013. (A and B) Monsoon index calculated as the average DJF (gridded) precipitation amount over the monsoon core region (-2.5 to -17.5°N, -47.5 to -72.5°E; as defined by Vuille et al., 2012). (C and D) Monsoon index based on the negative anomaly from climatological average of outgoing longwave radiation (OLR) spatially averaged over the monsoon core region (as defined by Vuille and Wagner, 2005). (E and F) Monsoon index calculated as vertical zonal wind shear (u_{850}-u_{250}) spatially averaged over the west tropical Atlantic Ocean (7.5 to -2.5°N, -20 to -45°E; as defined by Vuille and Werner, 2005). OLR and wind data from the Modern Era Retrospective analysis for Research and Applications. Representative precipitation gauge stations with close proximity to existing monsoon reconstructions (Fig. 1) and continuous coverage over the time period 1979-2013 were selected from the Global Historical Climate Network (stations: PEM00084673 [1], PEM00084686 [2], VE000080438 [3], BR038983570 [4], BR00E3-0520 [5]) and the Bank of Meteorological Data for Education and Research (station 83377 [6]).

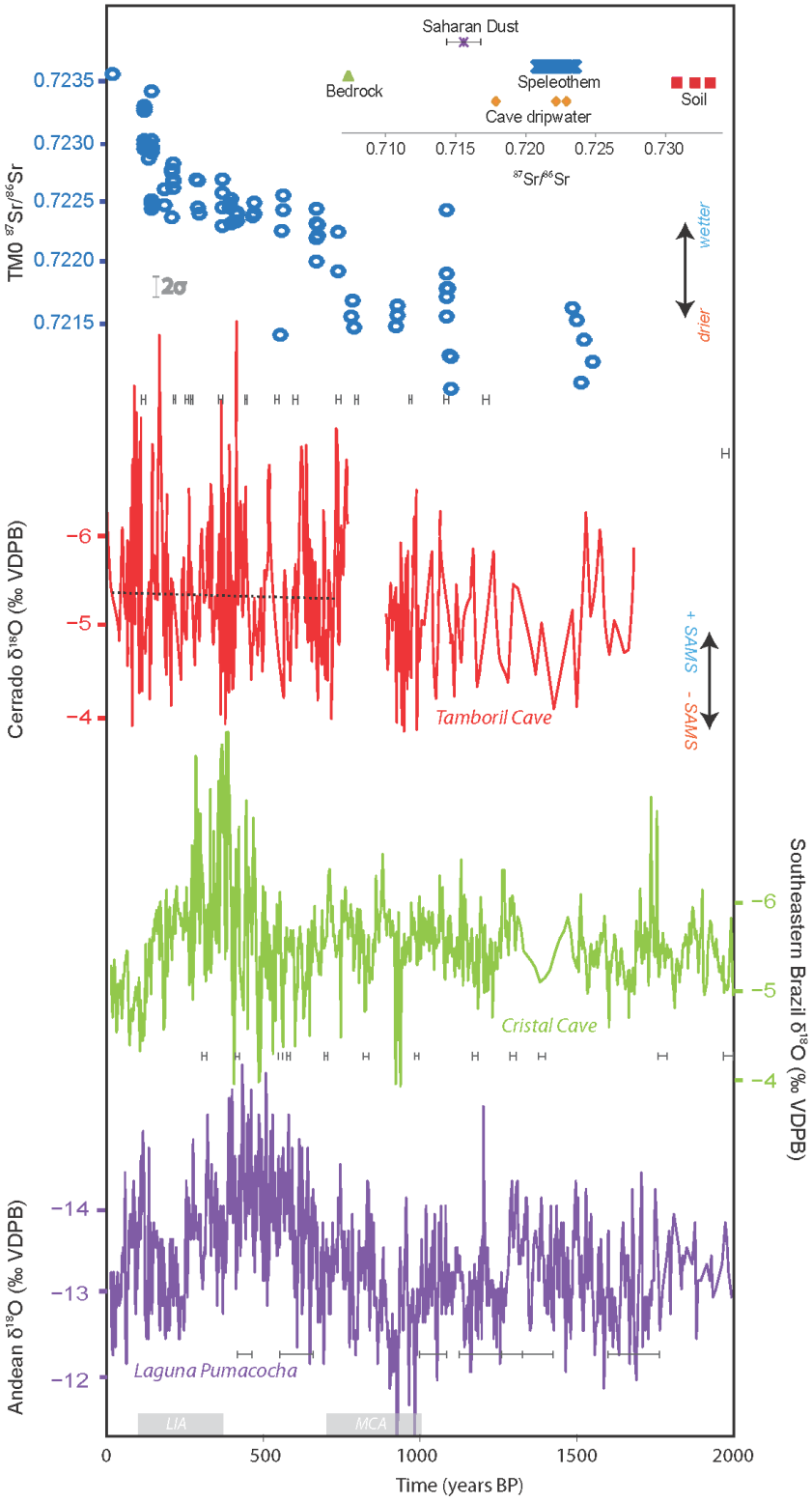
Saharan Dust
Bedrock
Speleothem
Soil
Cave dripwater
0.710
0.715
0.720
0.725
0.730
87Sr/86Sr
TM0 87Sr/86Sr
0.7235
0.7230
0.7225
0.7220
0.7215
2σ
wetter
drier
Cerrado δ18O (‰ VDPB)
−6
−5
−4
Tamboril Cave
+ SAMS
- SAMS
Cristal Cave
Southeastern Brazil δ18O (‰ VDPB)
−6
−5
−4
Andean δ18O (‰ VDPB)
−14
−13
−12
Laguna Pumacocha
LIA
MCA
0
500
1000
1500
2000
Time (years BP)

Figure 3: Time series of TM0 $^{87}Sr/^{86}Sr$ values along with variaions in $\delta^{18}O$ values in speleothems from Tamboril Cave and Cristal Cave (southeastern Brazil) and Laguna Pumachocha carbonate sediments (Peruvian Andes). TM0 $^{87}Sr/^{86}Sr$ values exhibit a substantial increasing trend over the last millennium (r = -0.88, one-tailed p = 0.00), whereas the trend in $\delta^{18}O$ does not increase over the last millenium (r = 0.02, one-tailed p = 0.31). $^{87}Sr/^{86}Sr$ values are shown for cave dripwater (n=3) and soils collected above Tamboril Cave (n=4) as well as the cave host rock, Bambui Group limestone (n=3; Misi et al., 2006), and Saharan dust collected in Barbados (Pourmand et al., 2014). U/Th age constraints are shows as gray bars (BP = years before 1950 C.E.). Little Ice Age (LIA; 700 to 1000 years BP) and Mideval Climate Anomaly (MCA; 250 to 450 years BP) shown as solid grey bars. The gap in the TM0 $\delta^{18}O$ record reflects an interval not sampled with respect to $\delta^{18}O$ (as opposed to a growth hiatus).

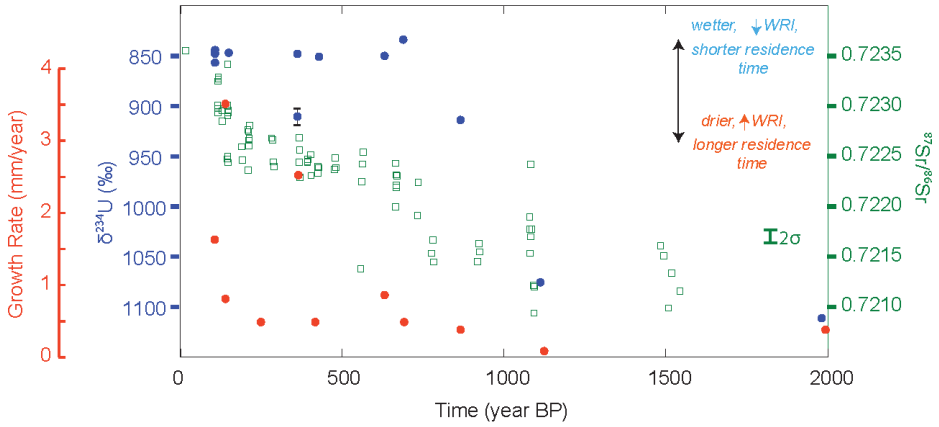

Figure 4: Comparison of TM0 $^{87}Sr/^{86}Sr$ to TM0 $\delta^{234}U$. TM0 $^{87}Sr/^{86}Sr$ (green squares) and $\delta^{234}U$ values (blue circles) corrected to their initial values. Uncertainty for $^{87}Sr/^{86}Sr$ analysis is shown by the green 2σ bar, uncertainty for most of the $\delta^{234}U$ is smaller than the marker size. Both moisture conditions sensitive proxies indicate an increase in local

moisture and changing moisture conditions. Growth rate (red circles) increases towards the present, potentially affecting speleothem $\delta^{234}U$ values. Note that the $\delta^{234}U$ axis is reversed for ease of interpretation (WRI = water rock interaction).

Supplementary Material

Sample collection

Soils were collected in one trench directly above the entrance of Tamboril Cave. The trench was dug using a combination of steel shovels and a hammer and chisel. Four samples were taken from the side of the trench at depth: 0-12 cm, 12-20 cm, 20-38 cm, and 38-49 cm (Table S1). Samples were stored in double walled Ziploc bags and shipped to the University of California, Davis (UCD).

Bedrock samples were collected within Tamboril Cave (n=1), on the entrance wall of Tamboril Cave (n=1) and in the nearby Tamboril River (n=2). Fresh bedrock samples were chipped off of the surface using a rock hammer. Bedrock within Tamboril Cave was only collected if it was considered to be host rock and not secondary, speleothem carbonate that could have been deposited after the cave formed. A bedrock sample was also collected from the entrance wall of the cave. These samples were stored in Ziploc bags and shipped to the UCD.

Sample preparation for analysis

Cave dripwaters were collected (July 28, 2015) throughout the cave by placing non-acid cleaned 250 ml low-density polyethylene bottles placed under chosen drip sites (n=4) throughout Tamboril Cave for 1-3 hours. A sampling blank was collected within Tamboril Cave by leaving a sampling bottle filled with nanopure water open in a dry area

of the cave for 3 hours. Upon collection, aliquots from each bottle were placed in separate 25 ml acid-cleaned polypropylene bottles and parafilmed for strontium analysis. Each original sample bottle was additionally parafilmed and refrigerated until shipped to UCD. After arrival on campus they were again refrigerated until analysis. Acidified aliquots of 8-15 ml of cave dripwaters were dried down in acid cleaned 7 ml snap-cap Teflon vials. The dried down portions of the dripwaters were brought up in 50 µl of 3N nitric acid and prepared for ion-exchange chemistry (Table S1).

Each soil sample was gently disaggregated prior to any chemical procedures to dislodge soil clumps. Approximately 1-2 grams of each sample was placed in a 15 ml acid-cleaned centrifuge tube. 5 ml of 1 M ammonium acetate, buffered to a pH of ~8, was added to each centrifuge tube. These tubes were shaken 3 times over a 30 minute span, and then centrifuged. The liquid was pipetted off each sample and placed in an acid-cleaned Teflon vial. This method was repeated twice, and soil residues were discarded after three total leaches with 1 M ammonium acetate. All liquid was dried down and brought up with 100 µl of 3N nitric acid and was process through ion-exchange chemistry.

Bedrock samples were prepared in three separate rounds for analysis. In the first round of analysis, chips of bedrock with fresh, un-weathered faces were used and disaggregated using a clean agate mortar and pestle. 3 to 4 mg of each bedrock sample were leached with 1 ml 4 % acetic acid for 3 to 4 hours in an acid cleaned 15 ml centrifuge tube at the Sedimentary Geochemistry Lab at UCD. Leachates were dried down and redissolved in 50 µl of 3N HNO3 and processed through ion exchange

chemistry using a peripump column procedure. In the second bedrock preparation, the same procedure as above was completed at the McGee Lab for Paleoclimate and Geochronology and process through ion exchange chemistry at the FIRST lab at Stony Brook University. Lastly, 340 mg of each bedrock sample was drilled from a fresh surface and split into 3 replicates and stored in microcentrifuge tubes. Two of the three replicates were leached with 1 ml 4% acetic acid and processed through ion exchange chemistry (standard gravity columns) at the Analytical Lab for Paleoclimate Studies at the University of Texas, Austin. One replicate was dissolved completely to determine the Sr budget of the whole rock.

Analytical methods

U-Th dating samples processed at MIT were prepared following methods detailed in Steponaitis et al. (2015). Samples weighing 2-50 mg were combined with a ^{229}Th-^{233}U-^{236}U tracer, digested, and purified via iron co-precipitation and ion exchange chromatography. Separate U and Th aliquots were analyzed using a Nu Plasma II-ES multi-collector ICP-MS equipped with a CETAC Aridus II desolvating nebulizer at MIT. Analyses were performed in static mode with ^{234}U and ^{230}Th measured on the ion counter and all other masses measured on Faraday cups, with U and Th standard solutions bracketing each analysis to monitor mass bias and ion counter yield. Tailing was assessed for each U sample by measurement of half-masses and mass 237. Th tailing was measured once per day. Corrections for procedural blanks were small, amounting to a maximum of 10 years in the ages of these samples. Corrections for initial ^{230}Th assumed an initial ^{230}Th/^{232}Th atomic ratio of $4.4 \pm 2.2 \times 10^{-6}$. Reported age uncertainties reflect

uncertainties from measurements, spike calibration, procedural blanks, SEM yield drift and tailing. Uncertainties on U and Th half-lives are not included, but would be insignificant relative to other uncertainties (Table S3).

Aragonite powders (~80μg) were subsampled from TM0 growth axis billets at 1.5 mm steps. This step size provided an average temporal resolution of 3 years, which was bin-averaged to the 25 year average temporal resolution of the $^{87}Sr/^{86}Sr$ record (Figure 2; Table S4). Samples were analyzed for $\delta^{18}O$ using a GVI Optima IRMS at UCD and a Thermo Finnegan MAT 253 with a Kiel Device at UT. Uncertainty for $\delta^{18}O$ analyses at UCD and UT are 0.07‰ and 0.05‰, respectively based on 64 replicate analysis of an internal standard (Silva et al. in prep).

Calculating monsoon indexes

The three modeling proxies for monsoon intensity used in this study were originally presented in Vuille and Werner (2005) and expanded upon in Vuille et al. (2012). We applied those methods to outputs from the Community Earth System Model Last Millennium Ensemble (CESM LME; Otto-Bleisner et al., 2015). The first of these is total precipitation over the monsoon core region (2.5 – 7.5°S, 45 - 75°W). This is calculated by adding total advective precipitation and total convective precipitation. The second monsoon index is Outgoing Longwave Radiation (OLR), which is affected by cloudiness and is therefore thought to be a proxy for convective activity. Vuille and Werner (2005) defined their convective OLR index as the negative DJF anomalies with respect to the annual cycle of OLR averaged over the monsoon core region, that convention is also used here. Finally, vertical wind shear is derived as the zonal wind anomalies (u850-u250)

over the region (7.5N–2.5°S, 45–20°W). The OLR and precipitation calculations were also applied to the SACZ region defined by Liebmann et al. (1999) (Fig.S4). Evapotranspiration is also evaluated using the CESM LME over the Cerrado region (15 to 22°S, 43 to 48°W).

Supplementary Figures

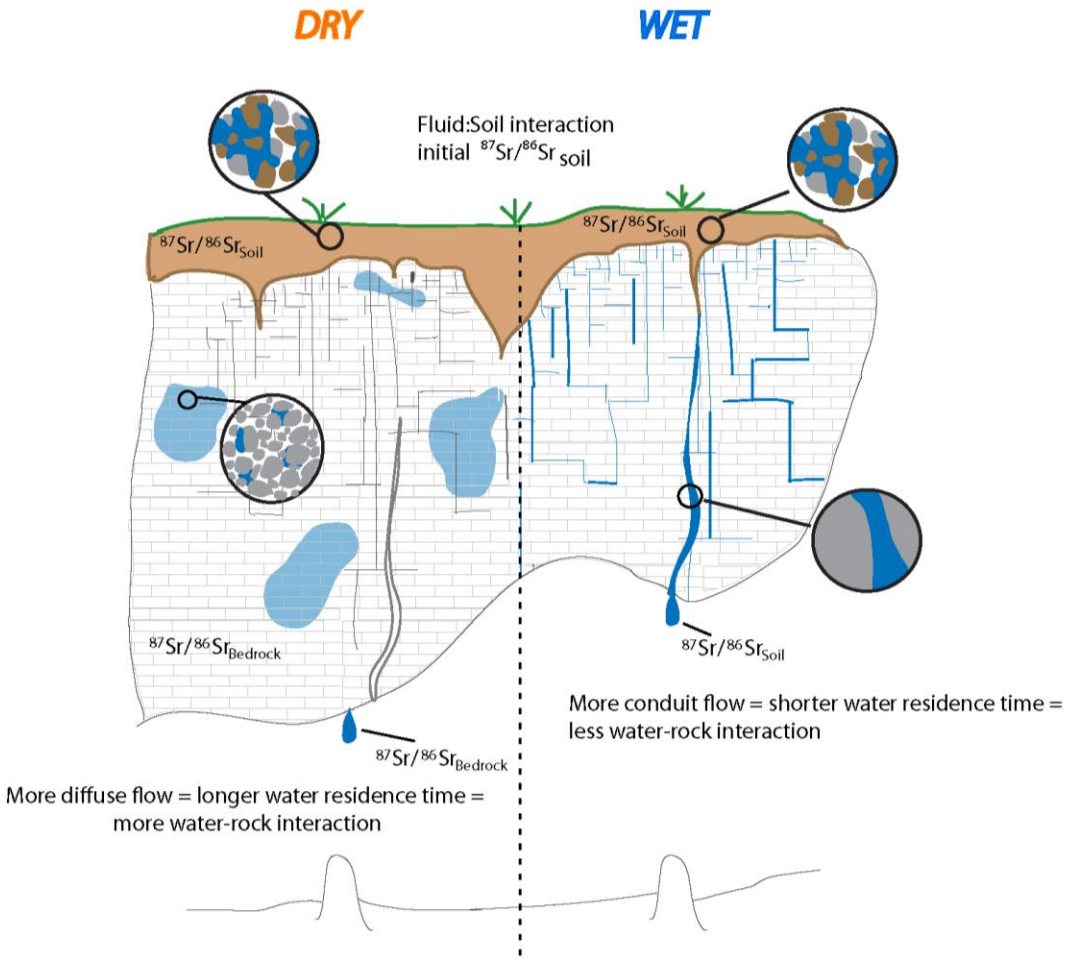

Supplementary Figure S1. Conceptual diagram of flow routing and dripwater Sr evolution during drier (left) vs. wetter (right) time periods.

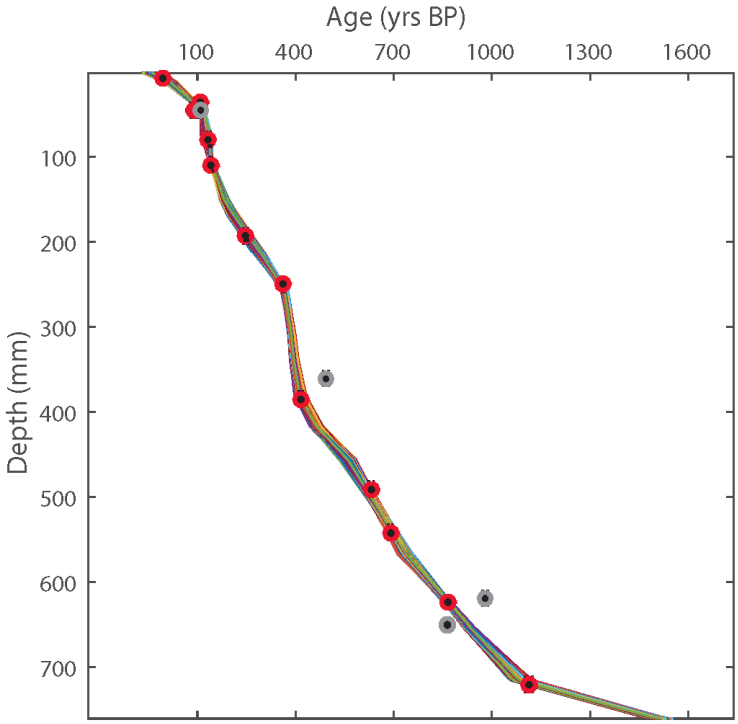

Supplementary Figure S2. Age to depth model using COPRA algorithm. Uncertainty on ages is smaller than the marker size. Red circles indicate data included in the age-depth model construction, gray circles indicate data that were not included in the age model.

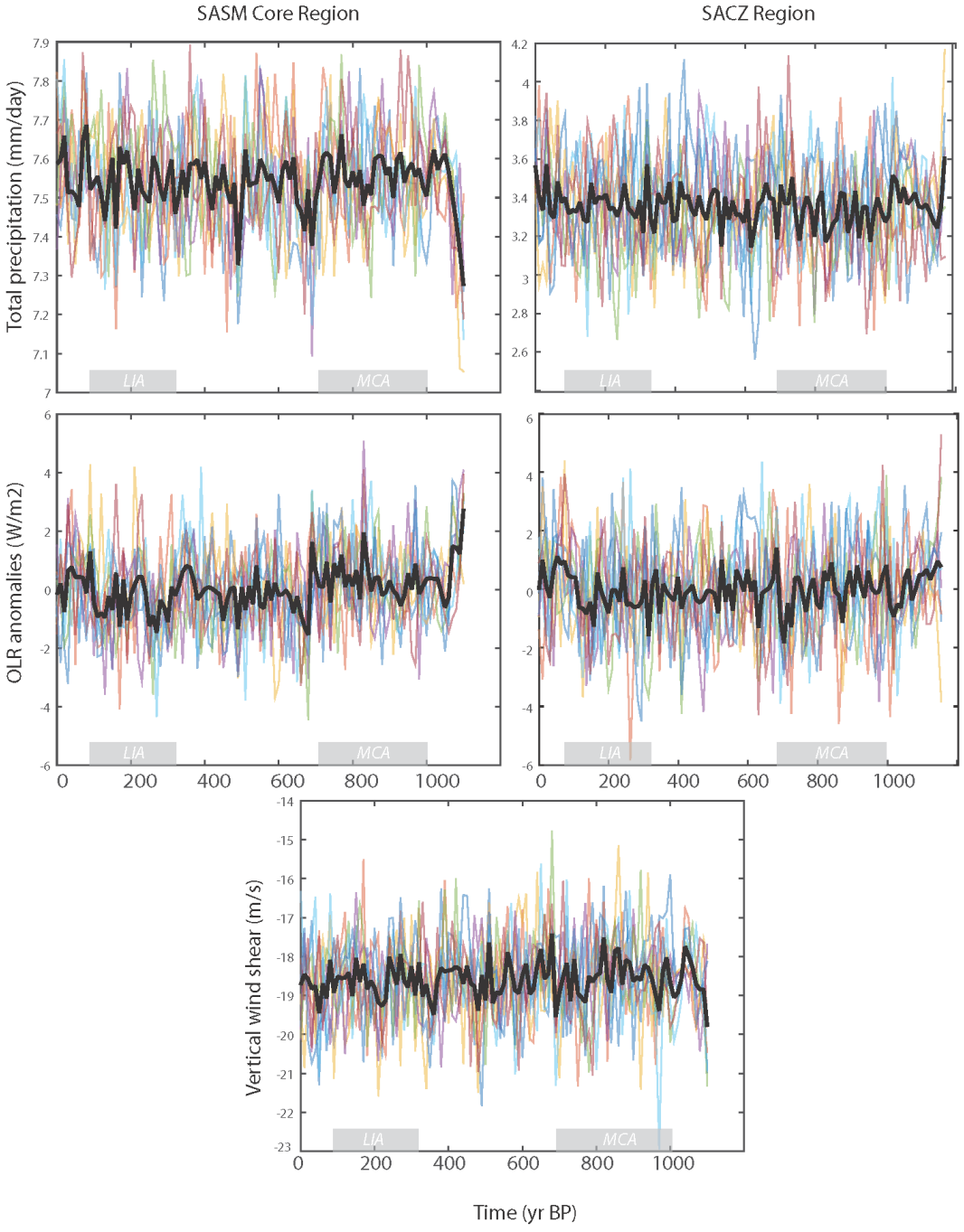
SASM Core Region
SACZ Region
Total precipitation (mm/day)
OLR anomalies (W/m2)
Vertical wind shear (m/s)
LIA
MCA
Time (yr BP)

Supplementary Figure S3. Time series of precipitation indices evaluated from the last millennium ensemble runs of the Community Earth System Model (Otto-Bleisner et al., 2015) for the SACZ region and the monsoon core.

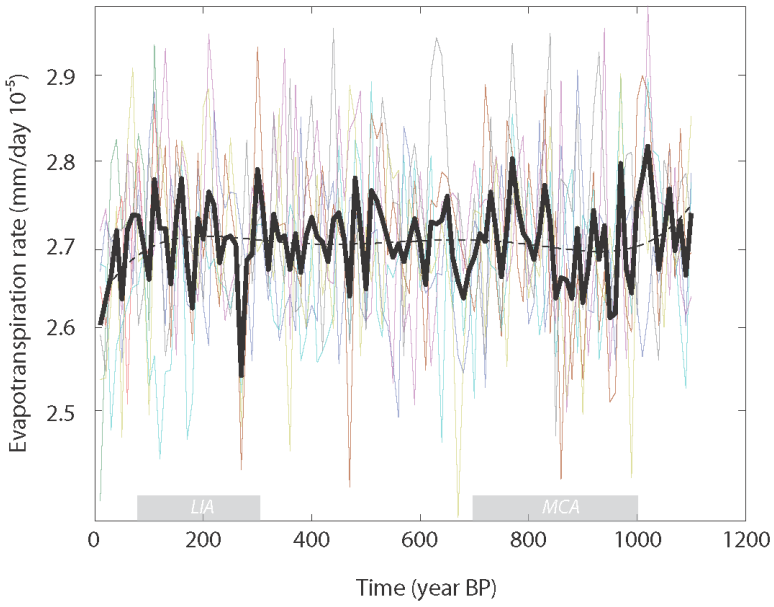

Supplementary Figure S4. Time series of evapotranspiration developed from the last millennium ensemble run of the Community Earth System Model for the Cerrado region.

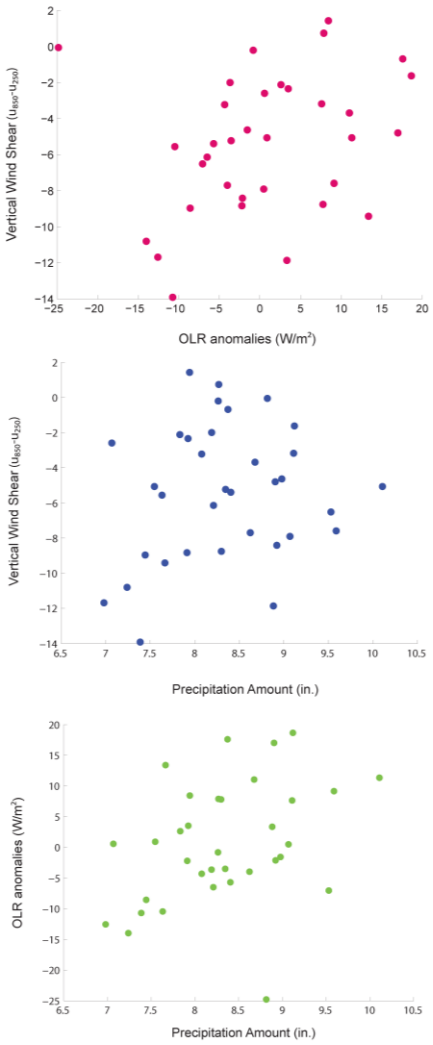

Supplementary Figure S5: Indices for monsoon strength are defined as OLR anomalies over the core region, precipitation amount over the core region, and vertical wind shear over the west tropical Atlantic Ocean. The precipitation index is significantly related to the OLR index (r = 0.36, one-tailed p = 0.02), but not to the vertical wind shear index (r =

0.17, one-tailed p = 0.16). The OLR index is significantly related to the vertical wind shear index (r = 0.28, one-tailed p = 0.05).

Supplementary Tables

Supplemental Table S1. Characterization of cave setting relative to Sr isotope compositions

Sample name	Sample Type	MC-ICP-MS 87Sr/86Sr	TIMS 87Sr/86Sr	Lab
Soil 0-12 cm	soil	0.7322		FIRST
Soil 12-20 cm	soil	0.7333		FIRST
Soil 20-38 cm	soil	0.7322		FIRST
Soil 38-49 cm	soil	0.7309		FIRST
				FIRST
TAM Rm 1	Cave dripwater	0.7230		FIRST
TAM Rm 3	Cave dripwater		0.72228	FIRST
TAM Rm 3 Drip 2	Cave dripwater		0.71800	FIRST

Supplemental Table S2. Speleothem Sr isotope values

Depth	Lab	MC-ICP-MS 87Sr/86Sr	TIMS 87Sr/86Sr	Method Difference
762.8	FIRST	0.7212	0.72122	-7.0E-05
761.9	FIRST		0.72116	
761	FIRST	0.7213		
760.3	FIRST	0.7210		
759.3	FIRST	0.7215		
758.6	FIRST	0.7216		
716.6	FIRST	0.7212		
716.3	FIRST	0.7209		
716	FIRST	0.7212		
713	UCD/ICPMS	0.72190		
713	UCD/ICPMS	0.72178		
714.5	FIRST	0.7218		
713.8	UCD/ICPMS	0.72242		
713.6	UCD/ICPMS	0.72170		
713.15	FIRST	0.7215		
652.5	FIRST	0.7215		
651.4	FIRST	0.7216	0.72168	-5.1E-05
649.2	FIRST	0.7215		
589.3	FIRST	0.7214		
588.3	FIRST	0.7217		
586.2	FIRST	0.7215		
567.7	FIRST	0.7222		
566.7	FIRST	0.7219		
525.8	FIRST	0.7223		
524.8	FIRST	0.7222	0.72230	-8.8E-05
523.6	FIRST	0.7223	0.72242	-1.1E-04
522.4	FIRST	0.7220		
523.7	FIRST	0.7222		
522.6	FIRST	0.7224	0.72250	-7.2E-05
456.3	FIRST	0.7225	0.72261	-6.5E-05
455.3	FIRST	0.7224	0.72248	-5.8E-05
454.2	FIRST	0.7222	0.72239	-1.4E-04
454.2	FIRST	0.7224	0.72244	-8.7E-05
453.1	FIRST	0.7214	0.72152	-1.4E-04
419	FIRST	0.7224	0.72245	-6.0E-05
418	FIRST	0.7225	0.72253	-4.8E-05
416.5	FIRST	0.7224		
381.8	FIRST	0.7224		
380.6	FIRST	0.7223		
379.4	FIRST	0.7224		
340.5	FIRST		0.72238	
339.3	FIRST	0.7223		

Depth	Lab	MC-ICP-MS 87Sr/86Sr	TIMS 87Sr/86Sr	Method Difference
338	FIRST	0.7225		
309.4	FIRST	0.7225		
308.5	FIRST	0.7224	0.72247	-3.2E-05
307.6	FIRST	0.7224	0.72248	-3.6E-05
259.75	FIRST	0.7223	0.72234	-5.0E-05
258.7	FIRST	0.7226		
257.6	FIRST	0.7224	0.72249	-4.9E-05
256.5	FIRST	0.7227		
213.8	FIRST	0.7224		
212.7	FIRST	0.7224	0.72249	-4.5E-05
211.6	FIRST	0.7227	0.72270	-4.2E-05
210.5	FIRST	0.7227		
169.1	UCD/ICPMS	0.72281		
168.6	UCD/ICPMS	0.72268		
168.1	UCD/ICPMS	0.72266		
167.6	UCD/ICPMS	0.72261		
166.5	FIRST	0.7227	0.72276	-1.6E-05
166.1	FIRST	0.7224	0.72258	-2.2E-04
165.4	UCD/ICPMS	0.72277		
151.4	FIRST	0.7225		
150.2	FIRST	0.7226	0.72262	-2.3E-05
104.7	FIRST	0.7224		
104.5	UCD/ICPMS	0.72294		
103.8	UCD/ICPMS	0.72296		
103.5	UCD/ICPMS	0.72290		
102.8	UCD/ICPMS	0.72342		
102.6	FIRST	0.7225		
102	FIRST	0.7225		
101.4	UCD/ICPMS	0.72301		
74.2	FIRST	0.7229	0.72288	-3.2E-05
73.1	FIRST	0.7230	0.72296	-5.1E-06
47.1	FIRST	0.7230		
46.3	FIRST	0.7229	0.72299	-6.3E-05
45.35	FIRST	0.7230		
49.1	FIRST	0.7233		
48.3	FIRST	0.7233		
47.2	FIRST	0.7232	0.72315	9.7E-05
11.5	FIRST	0.7236		
1	FIRST	0.7236		
Replicate analysis				
713	UCD/ICPMS	0.72190		
713	UCD/ICPMS	0.72178		

Depth	Lab	MC-ICP-MS 87Sr/86Sr	TIMS 87Sr/86Sr	Method Difference
	difference	1.2E-04		
454.2	FIRST	0.7222	0.72239	-1.4E-04
454.2	FIRST	0.7224	0.72244	-8.7E-05
	difference	1.1E-04		

Supplementary Table S3: U/Th dates for TM0

Sample ID	Depth (mm)	Chemistry Date	238U ng/g	± (2σ)	232Th pg/g	± (2σ)	δ234U per mil	± (2σ)	(230Th/238U) activity	± (2σ)	230Th/232Th ppm atomic	± (2σ)	Age (uncorr) yr	± (2σ)	Age (corr)* yr	± (2σ)	δ234U initial per mil	± (2σ)	Age (corr) yr BP	± (2σ)	Lab
BRZ8a	7	12/8/2014	1630	33	481	62	858.6	1.2	0.0010	0.0001	56	8	61	3	56.3	3.4	859	1.2	-9	3	MIT
BRZ8b	7	2/15/2015	1672	33	530	13	864.9	1.3	0.0011	0.0002	57	11	66	13	61.0	13.0	865	1.3	-4	13	MIT
BRZ9a	36	12/8/2014	2759	55	152	23	844.9	1.2	0.0029	0.0001	840	130	173	4	172.1	3.7	845	1.2	107	4	MIT
BRZ9b	36	12/30/2014	2479	50	105	45	843.8	1.4	0.0026	0.0001	990	430	156	4	155.5	3.9	844	1.4	91	4	MIT
BRZ9c	36	2/15/2014	2743	55	79	7	847.4	1.2	0.0026	0.0001	1410	140	151	7	150.2	7.3	848	1.2	86	7	MIT
BRZ B Top	79	11/23/2015	1351	27	745	17	846.6	1.4	0.0035	0.0001	102	2	209	3	199.8	5.7	847	1.4	134	6	MIT
BRZ B Bot	109	11/23/2015	2796	56	25	2	846.4	1.1	0.00353	0.00004	6262	572	209	2	208.4	2.2	847	1.1	142	2	MIT
BRZ11	250	12/30/2014	2841	57	84	3	847.1	1.4	0.0067	0.0001	3600	107	395	6	394.0	5.8	848	1.4	329	6	MIT
BRZ-6	385	11/23/2015	3703	74	297	7	847.6	1.1	0.00818	0.00010	1619	29	483	6	482.1	5.9	849	1.1	416	6	MIT
BRZ13	491	12/8/2014	4095	82	86	24	848.5	1.0	0.0118	0.0001	8900	2400	696	7	696.1	7.3	850	1.0	631	7	MIT
BRZ N	542	11/23/2015	3301	66	25	3	832.1	1.2	0.0127	0.0001	26770	2734	755	6	755.2	6.2	834	1.2	689	6	MIT
BRZP Top	624	11/9/2015	2233	45	183	4	911.3	1.2	0.0163	0.0001	3152	10	933	4	932.1	4.2	914	1.2	866	4	MIT
BRZ14	625	12/8/2014	2852	57	169	70	1128.7	1.1	0.0204	0.0002	5500	2300	1048	8.4	1047.5	8.4	1132	1.1	983	8	MIT
BRZP Bottom	657	11/9/2015	2487	50	8	0	985.8	1.2	0.0169	0.0001	80177	2242	930	5	930.4	5.4	988	1.2	865	5	MIT
BRZ15	721	12/30/2014	2589	52	65	2	1072.1	1.6	0.0223	0.0002	14200	370	1179	11	1178.0	11.0	1076	1.6	1113	11	MIT
BRZ tot Bot	790	11/9/2015	2159	43	104	2	1105.1	1.0	0.0392	0.0001	12996	29	2048	6	2047.8	6.4	1111	1.0	1982	6	MIT
BA-M1	193	4/1/2014	2073	41	762	15	910	10	0.0056	0.0001	242	2	318	6	312	7	911	9.8	248	7	UCD
BA-M2	360	4/1/2014	4968	99	414	8	842	3	0.0094	0.00014	1800	5	558	8	556	8	843	2.9	492	8	UCD
Interlab comparison analysis of sample splits from same horizons (BRZ9/10; BRZ 11/12)																					
BRZ10	36	10/8/2014	2569	52	68	1.4	856.4	2.6	0.0025	0.0000	761	20	145	4	144.6	3.6	857	2.6	145	4	BGC
BRZ12	250	10/8/2014	2477	50	28	0.6	849.9	2.9	0.0067	0.0001	4846	58	395	4	394.6	4.3	851	2.9	395	4	BGC

Notes: Corrected ages assume an initial 230Th/232Th of 4±2 ppm atomic; all 2sigma errors are given as absolutes; 0 BP = 1950; MIT - Mass. Institute of Tech.; BGC - Berkeley Geochronology Center; UCD - University of California Davis; Ages in grey were not used in construction of age model